

Low-field formation of room-temperature biskyrmions in centrosymmetric MnPdGa magnet

Cite as: Appl. Phys. Lett. **114**, 142404 (2019); <https://doi.org/10.1063/1.5089609>

Submitted: 21 January 2019 . Accepted: 27 March 2019 . Published Online: 11 April 2019

Xiaofei Xiao, Licong Peng, Xinguo Zhao , Ying Zhang , Yingying Dai , Jie Guo, Min Tong, Ji Li, Bing Li, Wei Liu, Jianwang Cai, Baogen Shen, and Zhidong Zhang



View Online



Export Citation



CrossMark

ARTICLES YOU MAY BE INTERESTED IN

[Large topological Hall effect in a geometrically frustrated kagome magnet Fe₃Sn₂](#)

Applied Physics Letters **114**, 192408 (2019); <https://doi.org/10.1063/1.5088173>

[Perspective: Magnetic skyrmions—Overview of recent progress in an active research field](#)

Journal of Applied Physics **124**, 240901 (2018); <https://doi.org/10.1063/1.5048972>

[Strain control of the Néel vector in Mn-based antiferromagnets](#)

Applied Physics Letters **114**, 142403 (2019); <https://doi.org/10.1063/1.5093701>

Lock-in Amplifiers

... and more, from DC to 600 MHz



Low-field formation of room-temperature biskyrmions in centrosymmetric MnPdGa magnet

Cite as: Appl. Phys. Lett. **114**, 142404 (2019); doi: [10.1063/1.5089609](https://doi.org/10.1063/1.5089609)

Submitted: 21 January 2019 · Accepted: 27 March 2019 ·

Published Online: 11 April 2019



View Online



Export Citation



CrossMark

Xiaofei Xiao,^{1,2} Licong Peng,³ Xinguo Zhao,^{1,2,a)}  Ying Zhang,^{3,4,b)}  Yingying Dai,^{1,2}  Jie Guo,^{1,2} Min Tong,¹ Ji Li,¹ Bing Li,^{1,2} Wei Liu,^{1,2} Jianwang Cai,³ Baogen Shen,³ and Zhidong Zhang^{1,2}

AFFILIATIONS

¹Shenyang National Laboratory for Materials Science, Institute of Metal Research, Chinese Academy of Sciences, Shenyang 110016, China

²School of Materials Science and Engineering, University of Science and Technology of China, Shenyang 110016, China

³Beijing National Laboratory for Condensed Matter Physics, Institute of Physics, Chinese Academy of Sciences, Beijing 100190, China

⁴Songshan Lake Materials Laboratory, Dongguan, Guangdong 523808, China

^{a)}Email: xgzhaoy@imr.ac.cn

^{b)}Email: zhangy@iphy.ac.cn

ABSTRACT

Magnetic skyrmions, a kind of localized spin texture topologically protected in magnetic materials, characterized by smaller size and much lower manipulating current density in comparison with ferromagnetic domain walls, are highlighted as potential information carriers for high-density magnetic storage devices. For technological applications, the stabilization of skyrmions in a temperature range around room temperature under a low magnetic field is essential. Here, we demonstrate the formation of magnetic biskyrmions in a low magnetic field at room temperature in a centrosymmetric hexagonal MnPdGa magnet *via* Lorentz transmission electron microscopy in combination with transport and magnetic measurements. High-density biskyrmions are generated at 300 K in a magnetic field of 0.15 T. In addition, biskyrmions can be generated from ferromagnetic domains and partly remained at zero field when the magnetic field is decreased. A large topological Hall resistivity is observed near room temperature. Furthermore, a wide temperature and magnetic-field window for biskyrmions is deduced from transport and magnetic properties. The simultaneous features of high-density and low magnetic field near room temperature in a single-component material make MnPdGa a promising candidate for future skyrmion-based topological spintronic applications.

Published under license by AIP Publishing. <https://doi.org/10.1063/1.5089609>

The demand for ever-increasing qualities and quantities of information carriers leads to the exploration of new technologies and materials. Magnetic skyrmions are promising because of their advantages such as high stability protected by topology, ultralow current density to manipulate, and small size.^{1,2} A magnetic skyrmion is a local whirl of the spin configuration, where the direction of spins wraps a unit sphere in not less than one time which is described by the topological skyrmion number.³ The formation of magnetic skyrmions originates from the competition between ferromagnetic exchange interactions and noncollinear interactions, such as dipolar interactions, Dzyaloshinskii-Moriya interactions (DMIs), frustrated exchange interactions, and four-spin exchange interactions.³ In the last decade, magnetic skyrmions were experimentally discovered or tailored in various materials or systems, for example, chiral magnets (MnSi,⁴ FeGe,⁵ GaV₄S₈,⁶ and Co-Zn-Mn alloys⁷), magnetic thin films with broken inversion symmetry (Fe/Ir,⁸ Pt/Co/Ta⁹), frustrated

magnets (Fe₃Sn₂¹⁰), artificial skyrmion systems (Co/Ni/Cu¹¹), anti-skyrmion materials (Mn_{1.4}PtSn¹²), and biskyrmion materials (La_{2-2x}Sr_{1+2x}Mn₂O₇,¹³ MnNiGa,¹⁴ and Cr₁₁Ge₁₉¹⁵). Among them, the magnetic biskyrmions, composed of two skyrmions with opposite spin helicities, are well-known for their tunable size and topological charges *via* the thickness, magnetic field, and electrical current.¹³ Biskyrmions are induced by the competition between dipolar interaction (demagnetization field energy) and magnetocrystalline anisotropy in the uniaxial ferromagnets with sufficiently strong easy-axis anisotropy.¹⁵

Lorentz transmission electron microscopy (LTEM) is favorable to observe skyrmions in real space because of its high resolution and rapid photography in recording magnetic domain structures.^{16,17} The topological Hall effect (THE), obtained by transport measurements, is regarded as additional experimental evidence for the existence of skyrmions. In metallic compounds, the topological spin arrangements of

skyrmions give rise to a fictitious emergent magnetic field, which rotates the conduction charges by Lorentz force, thus generating the THE.

For low-energy-consumption applications of skyrmions in spintronics, the existence of high-density skyrmions in a wider range of temperatures and magnetic fields, in particular for the operating temperature of room temperature or higher and the formation field of a lower field or even zero, is highly demanded. In earlier studies, most of the skyrmions were found to exist either at low temperatures in chiral magnets^{4,5,18} or in higher magnetic fields with low density at room temperature in Mn-based compounds.^{7,12,14} Although one can obtain high-density and nonvolatile zero-field room temperature biskyrmions in MnNiGa after electric current and field-cooling manipulations,^{19,20} the spontaneously high-density biskyrmions with a low formation field are demanded, which are demonstrated to exist in the Ni₂In-type hexagonal MnPdGa magnet.

A polycrystalline MnPdGa ingot was prepared by arc-melting in high-purity argon. Excess Mn (2 mol. %) over the stoichiometric composition was added to compensate for Mn losses during melting. The ingot was sealed in an evacuated quartz tube with argon gas, annealed at 1073 K for three days for homogeneity, and then quenched in ice water. The evolutionary behavior of biskyrmions was observed by using a JEOL JEM-2100F in the LTEM mode and a JEOL dedicated LTEM with an ultralow out-of-plane magnetic field. The magnetic field applied normal to the thin plate is induced by the magnetic objective lens of the microscope. The quantitative in-plane magnetization was analyzed by using the transport-of-intensity equation (TIE) method²¹ in the software package QPt with the defocus value of about 500 μm and a high pass of 3. For magnetization and transport measurements, a bar-shape sample was polished to a size of about $6 \times 2 \times 0.4 \text{ mm}^3$. The transport and magnetic properties of this sample were measured using a Physical Property Measurement System (PPMS, Quantum Design Inc.) and a Magnetic Property Measurement System (MPMS, Quantum Design Inc.), respectively. The Hall and the longitudinal resistivity were almost simultaneously measured using a standard four-probe method. The field dependence of the Hall resistivity was obtained after subtracting the longitudinal-resistivity component. The amplitude and frequency in the alternating-current (AC) susceptibility measurements are 0.0003 T and 10 Hz, respectively.

Powder X-ray diffraction patterns show that the as-prepared sample crystallizes in the Ni₂In-type hexagonal structure (space group $P6_3/mmc$) (see Fig. S1 of the [supplementary material](#)), which is consistent with Ref. 22. Here, we focus on MnPdGa because it exhibits the lowest Néel temperature (T_N) and almost the highest Curie temperature (T_C) in (Mn_{1-x}Pd_x)₂Ga (with $0.3 \leq x < 0.6$) compounds.²² According to neutron-diffraction results,²² all 2(a) sites are occupied by Mn atoms, the 2(d) sites by Pd and residual Mn atoms, and the 2(c) sites by Ga atoms in off-stoichiometric Mn-Pd-Ga compounds. At temperatures below T_N , an antiferromagnetic (AFM) component lying in the basal plane originates from the canted spin structure of Mn at the 2(a) sites, while the ferromagnetic component is parallel to the c axis. The temperature dependence of the AC susceptibility is shown in Fig. S2 of the [supplementary material](#). The real part of the susceptibility increases with increasing temperature until $T_N = 138 \text{ K}$ and abruptly drops at $T_C = 308 \text{ K}$. The values of T_N and T_C are in good agreement with published data.²²

Figure 1 shows the under-focused LTEM images at 300 K of a MnPdGa thin plate. The evolution of skyrmions from stripe domains

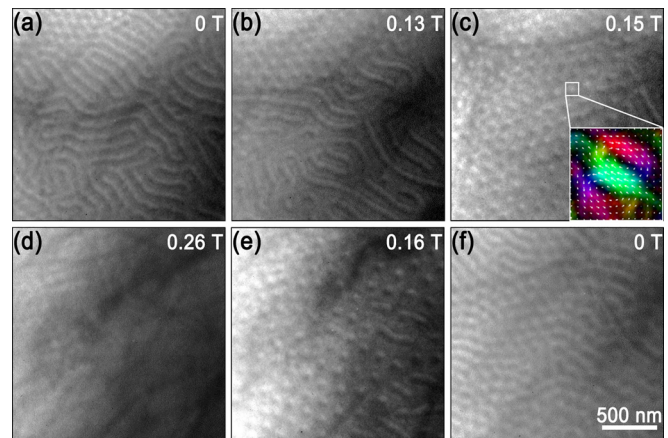


FIG. 1. Under-focused LTEM images of the skyrmion evolution at different magnetic fields at 300 K for a MnPdGa grain along the [001] zone axis. The perpendicular magnetic field increased to saturate the domains to the ferromagnetic state and then decreased back to zero. (a) At zero field, some skyrmions exist besides the majority stripes. (b) A lot of stripes transform to skyrmions at 0.13 T. (c) Complete skyrmion lattice at 0.15 T. As shown in the inset, the corresponding in-plane magnetization-distribution map of a selected skyrmion is confirmed to be a biskyrmion. The color map and white arrows represent the magnetization direction at each point. (d) Saturated ferromagnetic state at 0.26 T. (e) Reformation of skyrmions when the field is decreased to 0.16 T. (f) Some skyrmions remain upon the majority stripes at zero field.

is common except for the relatively low critical magnetic field and the appearance of residual skyrmions after removing the magnetic field. The magnetic domains in the grain along the [001] zone axis are found to be stripes with a periodicity of about 100 nm at zero field [Fig. 1(a)]. The existence of some skyrmions at the remnant magnetic field of the common objective lens indicates that the formation field of skyrmions in MnPdGa is low. Upon increasing the magnetic field up to 0.13 T, a lot of skyrmions are generated from the stripes [Fig. 1(b)]. Almost all stripes transform to the skyrmion lattice when the field increases to 0.15 T, and the skyrmion density is estimated to be about $60/\mu\text{m}^2$ [Fig. 1(c)]. The skyrmions vanish when the magnetic field increases up to 0.26 T, as shown in Fig. 1(d). The LTEM image without significant contrast indicates a field-induced spin-collinear ferromagnetic (FM) state. When the magnetic field is decreased, skyrmions reappear at about 0.16 T [Fig. 1(e)]. The reversible skyrmion formation from the FM state in the decreasing field is rarely observed and is in contrast to the abrupt appearance of stripes from the FM state in previously investigated skyrmion materials.²³ Some skyrmions remain upon the majority stripes due to the remnant magnetic field of about 0.03 T after switching off the objective-lens current [Fig. 1(f)]. The skyrmions observed here have biskyrmionic spin configurations, as shown in the inset of Fig. 1(c). Compared to the previous studies on classic skyrmions in chiral magnets⁷ or biskyrmions in other Mn-based materials,^{13,14} MnPdGa presents simultaneous advantages of both the high density and the lower formation field at room temperature. The high density may be associated with the proper competition of different interactions and energies near T_C , which is commonly observed in previously skyrmion-hosting materials such as Co-Zn-Mn alloy and MnNiGa.^{7,20} The lower formation field may be ascribed to the appropriate easy-axis anisotropy in the hexagonal structure.¹⁵ The required

lower magnetic field to stabilize skyrmions in the MnPdGa magnet saves energy and indicates potential for skyrmion-device applications.

LTEM images (Fig. 2) show similar stripe domains at different temperatures below T_C , indicating that biskyrmions will be generated from the stripe state under the magnetic field at low temperatures. The wide temperature range of skyrmions formation is further confirmed by the measurements of transport and magnetic properties. Figure 3(a) illustrates the perpendicular longitudinal magnetoresistance (MR), $(\rho_{xx}(H) - \rho_{xx}(0))/\rho_{xx}(0)$, over the temperature range of 10–310 K. It is interesting to note that MR shows different dependences on the magnetic field at different temperatures. MR increases at first and then decreases with the increasing magnetic field at temperatures below T_N , whereas it decreases monotonously above T_N . The former may be induced by the AFM component of the canted spins, and the latter is common in metallic ferromagnets which is attributed to the damping of spin waves by the magnetic field, leading to a decrease in the scattering of electrons by spin waves.²⁴ There is no clear kink in the MR curves, which differs from many other skyrmion-hosting materials.^{10,14,25,26}

The Hall resistivity (ρ_{xy}) shows a positive and linear proportionality to the magnetic field at high fields, but a complex relation at low fields [Fig. 3(b)]. In metallic skyrmion-hosting materials, the THE exists in a magnetic field range where skyrmions are supported. The Hall resistivity can usually be separated into three parts: the linear-field-dependent normal Hall effect (ρ_{xy}^N), the magnetization-induced anomalous Hall effect (ρ_{xy}^A), and the THE (ρ_{xy}^T), which has the relation of $\rho_{xy} = \rho_{xy}^N + \rho_{xy}^A + \rho_{xy}^T = R_0\mu_0H + S_A\rho_{xx}^2M + \rho_{xy}^T$, where R_0 is the normal Hall coefficient, μ_0H the perpendicular magnetic field, $S_A\rho_{xx}^2$ the anomalous Hall coefficient, and M the magnetization. Generally, S_A is supposed to be field independent when $\rho_{xy} \ll \rho_{xx}$ ^{27,28} and this condition is fulfilled in the present measurements because ρ_{xx} is two orders of magnitude larger than ρ_{xy} . When the magnetic field exceeds

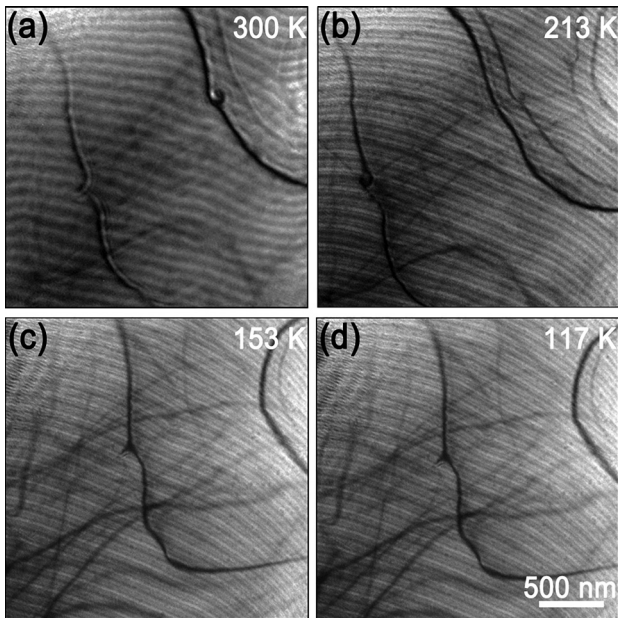


FIG. 2. Stripe domains of MnPdGa at temperatures from 300 K to 117 K at zero magnetic field.

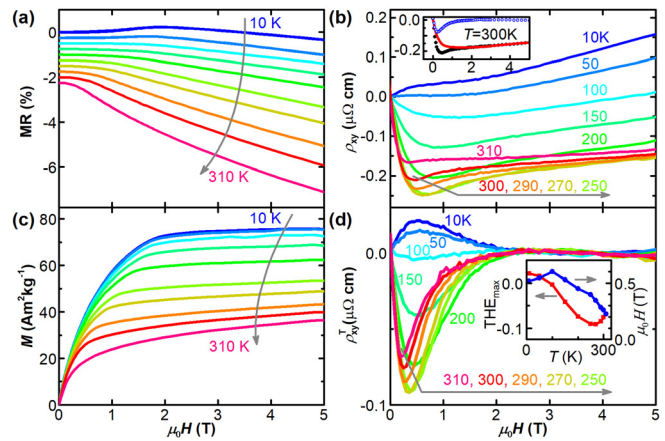


FIG. 3. Topological Hall resistivity (ρ_{xy}^T) of a polycrystalline MnPdGa bar at 10–310 K. The applied magnetic field varies from 5 T to -5 T and back to 5 T, but only half of the data are shown because of the symmetry. (a) Magnetoresistivity (MR) vs applied magnetic field (shifted vertically by a step of -0.25% for clarity). (b) Hall resistivity (ρ_{xy}). The representative calculation of ρ_{xy}^T at 300 K is shown in the inset, where the black solid dots are the experimental data, the red line is the fitted curve of $R_0\mu_0H + S_A\rho_{xx}^2M$, and the blue open circles represent the derived ρ_{xy}^T . (c) Magnetization (M). (d) ρ_{xy}^T . The inset shows the temperature dependence of the maximum amplitude of ρ_{xy}^T and the corresponding field.

a critical value (H_C), all skyrmions transform to FM and the THE disappears. Therefore, R_0 and S_A can be determined as the slope and intercept of the linear-fitting curve of ρ_{xy}/μ_0H vs ρ_{xx}^2M/μ_0H above H_C , respectively. The $M(H)$ curves show a hard-axis behavior without hysteresis due to the strong shape anisotropy of the bar-shape sample [Fig. 3(c)]. The saturation behavior at low temperatures indicates that the moment of the AFM component lying in the basal plane is much smaller than that of the FM along the c axis. The saturation magnetization (M_S) and magnetocrystalline anisotropy energy (K_U) were calculated by using the law of approach to saturation.²⁹ Both the M_S and the K_U values decrease with increasing temperature, and the ratio of the anisotropy energy and the demagnetization field energy [$K_U/(\mu_0M_S^2/2)$] comes to 1.29–1.45. This ratio value, which is required to be greater than 1 to form magnetic bubbles and skyrmions,¹⁵ is sufficient to support biskyrmions in MnPdGa. We obtain the topological Hall resistivity by subtracting the normal Hall effect and the anomalous Hall effect from the measured Hall resistivity with the parameters R_0 and S_A obtained from a good fit in the high fields [Fig. 3(d)]. A representative calculation at 300 K is shown in the inset of Fig. 3(b), and calculations at more temperatures are shown in Fig. S3 of the supplementary material. The fitted parameters R_0 and S_A change abruptly with temperature around T_N (see Fig. S4 of the supplementary material). With decreasing temperature, R_0 increases significantly below T_N , suggesting a decreasing effective carrier density. The positive R_0 indicates hole-like conduction. The almost constant S_A at $T > T_N$ is consistent with conventional theories which consider S_A to be proportional to the spin-orbit interaction and independent of temperature in ferromagnets.³⁰ The strong variation of both R_0 and S_A below T_N is possibly due to the variation of the magnetic structure, similar to the situation of antiferromagnetic Mn_5Si_3 , which shows a large THE at low temperatures.³¹

As shown in Fig. 3(d), the topological Hall resistivity significantly changes with temperatures. At 100 K, no sharp THE peak but a broad one is found, whereas clear peaks show positive values below 100 K and negative values above this temperature. The magnetic field where the maximum amplitude of the THE locates has a maximum at about T_N and the maximum amplitude of the THE exhibits a large value (of about $-0.09 \mu\Omega \text{ cm}$) around room temperature [inset of Fig. 3(d)]. The large THE, which indicates the existence of skyrmions with high-density, is beneficial for the potential method of electrical detection of skyrmions. That the THE exists even at zero field can be attributed to the partly remaining of biskyrmions at zero field, as observed in LTEM.

It is interesting to note that the THE changes its sign at about 100 K. According to previous reports, the sign of the THE can be affected by the shape of materials and variation of the magnetic field and temperature. For instance, the THE is positive in MnNiGa bulk, but negative in the film.^{14,26} Besides, the change in the THE sign in MnGe with the increasing field may possibly originate from the short-period skyrmion-antiskyrmion cubic lattice.^{18,27} In MnSi film, the sign of the THE changes below 5 K, which is attributed to the variation of the spin polarization by tensile strain or temperature fluctuation.³² In the present MnPdGa sample, the spin textures at low temperatures are different from that at room temperature because of the AFM component in the basal plane below 138 K.²² Similar to the THE in a noncollinear antiferromagnet,³¹ the AFM of canted spins can give rise to a THE (THE_{AFM}), which may have an opposite sign to the THE induced by biskyrmions (THE_{BS}), and thus, the total THE (THE_{tot}) will be cancelled out partially. The decrease in (the absolute value of) THE_{BS} with temperature decreasing from 250 K to 150 K can be ascribed to a reduction of biskyrmion density, similar to that in MnNiGa.¹⁴ As the temperature decreases to T_N (138 K), THE_{AFM} arises besides THE_{BS} . Upon further decreasing temperature, THE_{AFM} increases and THE_{BS} (absolute value) decreases, and thus, THE_{tot} crosses zero and changes its sign. The spin textures at lower temperatures need to be confirmed by further experiments.

To determine the critical fields of transformation between different spin textures, the AC susceptibility has been measured as a function of the direct-current (DC) magnetic field in the temperature range of 10–300 K. The normalized AC susceptibility, $\chi'(H)/\chi'(0)$, decreases monotonically with the increasing magnetic field and shows a hump (Fig. 4). As shown in the inset, there are three kinks in the derivative of susceptibility over the field $d\chi'/dH$ curve, corresponding to the critical fields: H_{C1} , biskyrmion lattice (SkX) beginning to generate from the stripe-domain (S) or spin-canted (C) state; H_{C2} , pure SkX without S or C; H_{C3} , transformation from SkX to FM. This transformation process is consistent with that observed at 300 K by means of LTEM. Due to the different ground states, the trends of the critical fields with temperatures show a turning point around T_N . Combining the THE results with the critical fields, a magnetic phase diagram has been derived as plotted in Fig. S5 of the [supplementary material](#). The THE shows maximum absolute values in the field range where SkX is stable. To investigate the MnPdGa magnet further, a large monocrystalline MnPdGa is needed, which we will attempt to grow in the future.

In summary, high-density biskyrmions in a low magnetic field are identified at room temperature in MnPdGa by direct observation using LTEM and by a large THE derived from transport and magnetic

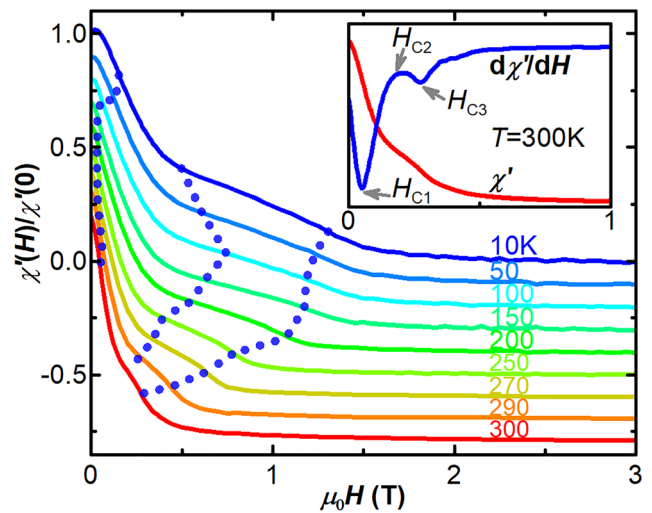


FIG. 4. Temperature dependence of the normalized AC susceptibility. The data at different temperatures were shifted vertically by a step of 0.1 for clarity. The dotted lines indicate the three critical fields, which is determined as the kinks of the first derivative of the susceptibility, as shown in the inset.

measurements. It is found that biskyrmions can be generated from ferromagnetic domains and partly remained at zero field when the magnetic field is decreased. In polycrystalline MnPdGa, biskyrmions can be stabilized in a temperature range of 10–308 K at different magnetic fields, as deduced from transport and magnetic measurements. Below T_N , the THE changes its sign because of the coexistence of canted spins and biskyrmions. The simultaneous features of high skyrmion density and low magnetic field near room temperature in a single-component material make MnPdGa a promising candidate for future skyrmion-based topological spintronic applications. Recently, it was reported that the LTEM images of biskyrmions can be explained as conventional type-II bubbles with topological charge 0 (no THE exists),³³ besides the topological nontrivial biskyrmions. Based on the large THE observed in our MnPdGa magnet, the LTEM images were induced by biskyrmions with topological charge 2.

See [supplementary material](#) for the figure of XRD pattern, temperature dependence of the AC susceptibility, calculation of topological Hall resistivity at different temperatures, temperature dependence of the fitted parameters R_0 and S_A , and magnetic phase diagram of a bulk polycrystalline MnPdGa.

This work was supported by the National Key Research and Development Program of China (Grant Nos. 2016YFB0700901 and 2016YFB0700902), the National Natural Science Foundation of China (Grant Nos. 51571194, 51771197, and 51701217), the Chinese Academy of Sciences (Grant No. KJZD-EW-M05), and the Youth Innovation Promotion Association, CAS, 2015004.

REFERENCES

- ¹A. Fert, N. Reyren, and V. Cros, *Nat. Rev. Mater.* **2**, 17031 (2017).
- ²N. Kanazawa, S. Seki, and Y. Tokura, *Adv. Mater.* **29**, 1603227 (2017).
- ³N. Nagaosa and Y. Tokura, *Nat. Nanotechnol.* **8**, 899 (2013).

- ⁴S. Mühlbauer, B. Binz, F. Jonietz, C. Pfleiderer, A. Rosch, A. Neubauer, R. Georgii, and P. Böni, *Science* **323**, 915 (2009).
- ⁵S. X. Huang and C. L. Chien, *Phys. Rev. Lett.* **108**, 267201 (2012).
- ⁶I. Kézsmárki, S. Bordács, P. Milde, E. Neuber, L. M. Eng, J. S. White, H. M. Rønnow, C. D. Dewhurst, M. Mochizuki, K. Yanai, H. Nakamura, D. Ehlers, V. Tsurkan, and A. Loidl, *Nat. Mater.* **14**, 1116 (2015).
- ⁷Y. Tokunaga, X. Z. Yu, J. S. White, H. M. Rønnow, D. Morikawa, Y. Taguchi, and Y. Tokura, *Nat. Commun.* **6**, 7638 (2015).
- ⁸N. Romming, C. Hanneken, M. Menzel, J. E. Bickel, B. Wolter, K. von Bergmann, A. Kubetzka, and R. Wiesendanger, *Science* **341**, 636 (2013).
- ⁹S. Woo, K. Litzius, B. Krüger, M. Y. Im, L. Caretta, K. Richter, M. Mann, A. Krone, R. M. Reeve, M. Weigand, P. Agrawal, I. Lemesch, M. A. Mawass, P. Fischer, M. Kläui, and G. S. D. Beach, *Nat. Mater.* **15**, 501 (2016).
- ¹⁰Z. P. Hou, W. J. Ren, B. Ding, G. Z. Xu, Y. Wang, B. Yang, Q. Zhang, Y. Zhang, E. K. Liu, F. Xu, W. H. Wang, G. H. Wu, X. X. Zhang, B. G. Shen, and Z. D. Zhang, *Adv. Mater.* **29**, 1701144 (2017).
- ¹¹J. Li, A. Tan, K. W. Moon, A. Doran, M. A. Marcus, A. T. Young, E. Arenholz, S. Ma, R. F. Yang, C. Hwang, and Z. Q. Qiu, *Nat. Commun.* **5**, 4704 (2014).
- ¹²A. K. Nayak, V. Kumar, T. P. Ma, P. Werner, E. Pippel, R. Sahoo, F. Damay, U. K. Rößler, C. Felser, and S. S. P. Parkin, *Nature* **548**, 561 (2017).
- ¹³X. Z. Yu, Y. Tokunaga, Y. Kaneko, W. Z. Zhang, K. Kimoto, Y. Matsui, Y. Taguchi, and Y. Tokura, *Nat. Commun.* **5**, 3198 (2014).
- ¹⁴W. H. Wang, Y. Zhang, G. Z. Xu, L. C. Peng, B. Ding, Y. Wang, Z. P. Hou, X. M. Zhang, X. Y. Li, E. K. Liu, S. G. Wang, J. W. Cai, F. W. Wang, J. Q. Li, F. X. Hu, G. H. Wu, B. G. Shen, and X. X. Zhang, *Adv. Mater.* **28**, 6887 (2016).
- ¹⁵R. Takagi, X. Z. Yu, J. S. White, K. Shibata, Y. Kaneko, G. Tatara, H. M. Rønnow, Y. Tokura, and S. Seki, *Phys. Rev. Lett.* **120**, 037203 (2018).
- ¹⁶X. Z. Yu, Y. Onose, N. Kanazawa, J. H. Park, J. H. Han, Y. Matsui, N. Nagaosa, and Y. Tokura, *Nature* **465**, 901 (2010).
- ¹⁷A. Tonomura, X. Z. Yu, K. Yanagisawa, T. Matsuda, Y. Onose, N. Kanazawa, H. S. Park, and Y. Tokura, *Nano Lett.* **12**, 1673 (2012).
- ¹⁸T. Tanigaki, K. Shibata, N. Kanazawa, X. Z. Yu, Y. Onose, H. S. Park, D. Shindo, and Y. Tokura, *Nano Lett.* **15**, 5438 (2015).
- ¹⁹L. C. Peng, Y. Zhang, M. He, B. Ding, W. H. Wang, H. F. Tian, J. Q. Li, S. G. Wang, J. W. Cai, G. H. Wu, J. P. Liu, M. J. Kramer, and B. G. Shen, *npj Quantum Mater.* **2**, 30 (2017).
- ²⁰L. C. Peng, Y. Zhang, W. H. Wang, M. He, L. L. Li, B. Ding, J. Q. Li, Y. Sun, X. G. Zhang, J. W. Cai, S. G. Wang, G. H. Wu, and B. G. Shen, *Nano Lett.* **17**, 7075 (2017).
- ²¹K. Ishizuka and B. Allman, *J. Electron Microscop.* **54**, 191 (2005).
- ²²H. Shiraishi, T. Hori, N. Ohkubo, K. Ohoyama, and Y. Yamaguchi, *J. Appl. Phys.* **93**, 6996 (2003).
- ²³D. Morikawa, X. Z. Yu, K. Karube, Y. Tokunaga, Y. Taguchi, T. H. Arima, and Y. Tokura, *Nano Lett.* **17**, 1637 (2017).
- ²⁴B. Raquet, M. Viret, E. Sondergard, O. Cespedes, and R. Mamy, *Phys. Rev. B* **66**, 024433 (2002).
- ²⁵K. Kadowaki, K. Okuda, and M. Date, *J. Phys. Soc. Jpn.* **51**, 2433 (1982).
- ²⁶B. Ding, Y. Q. Li, G. Z. Xu, Y. Wang, Z. P. Hou, E. K. Liu, Z. Y. Liu, G. H. Wu, and W. H. Wang, *Appl. Phys. Lett.* **110**, 092404 (2017).
- ²⁷N. Kanazawa, Y. Onose, T. Arima, D. Okuyama, K. Ohoyama, S. Wakimoto, K. Kakurai, S. Ishiwata, and Y. Tokura, *Phys. Rev. Lett.* **106**, 156603 (2011).
- ²⁸M. Lee, Y. Onose, Y. Tokura, and N. P. Ong, *Phys. Rev. B* **75**, 172403 (2007).
- ²⁹G. Hadjipanayis, D. J. Sellmyer, and B. Brandt, *Phys. Rev. B* **23**, 3349 (1981).
- ³⁰N. Nagaosa, J. Sinova, S. Onoda, A. H. MacDonald, and N. P. Ong, *Rev. Mod. Phys.* **82**, 1539 (2010).
- ³¹C. Stürgers, G. Fischer, P. Winkel, and H. V. Löhneysen, *Nat. Commun.* **5**, 3400 (2014).
- ³²Y. F. Li, N. Kanazawa, X. Z. Yu, A. Tsukazaki, M. Kawasaki, M. Ichikawa, X. F. Jin, F. Kagawa, and Y. Tokura, *Phys. Rev. Lett.* **110**, 117202 (2013).
- ³³J. C. Loudon, A. C. Twitchett-Harrison, D. Cortés-Ortuño, M. T. Birch, L. A. Turnbull, A. Štefančič, F. Y. Ogrin, E. O. Burgos-Parra, N. Bukin, A. Laurenson, H. Popescu, M. Beg, O. Hovorka, H. Fangohr, P. A. Midgley, G. Balakrishnan, and P. D. Hatton, “Do images of biskyrms show Type-II bubbles?” *Adv. Mater.* (published online).